



Modeling and compensation of comprehensive errors for thin-walled parts machining based on on-machine measurement

Zhengchun Du¹ · Guangyan Ge¹ · Yukun Xiao¹ · Xiaobing Feng¹ · Jianguo Yang¹

Received: 8 February 2021 / Accepted: 1 June 2021 / Published online: 9 June 2021
© The Author(s), under exclusive licence to Springer-Verlag London Ltd., part of Springer Nature 2021

Abstract

Thin-walled parts are widely applied in the automotive and aerospace industry for their superior properties. However, severe machining error may occur due to their low rigidity under the effects of multiple error sources in the machining process. Solutions based on mechanism analysis and finite element method have been developed while most of them are not robust under the complex machining conditions. Aiming to solve this problem, a comprehensive error compensation method that includes three major error sources, which are geometric error, thermal error, and force-induced error, is proposed. The geometric error and thermal-induced error of the machining center are firstly modeled and compensated to provide a high precision movement system for the on-machine measurement inspection. The force-induced error model is then established based on the probing data. Finally, the comprehensive error model is obtained through the transformation of the coordinate systems. Besides, a real-time compensation system is developed based on the specific functions of the NC system. To validate the proposed method, two sets of compensation cases are conducted, the objects of which are a thin web workpiece and a valve body part, respectively. The experiment results reveal that the machining errors of both experiment sets are decreased by more than 60.7% and the machining productivity is improved by more than 41.9%.

Keywords Thin-walled parts · Comprehensive error · Error compensation · On-machine measurement

1 Introduction

Thin-walled parts, such as valve body and thin web parts, are widely applied in automotive and aerospace industries due to their superior properties of high strength-to-weight ratio, compact structure, and lightweight [1]. However, the low rigidity of thin-walled parts causes workpiece deflection under cutting forces or clamping forces, which often leads to low machining accuracy. Besides, geometric error and thermal-induced error of the machine tool itself also play vital roles in the final machining accuracy. The above three error sources constitute a high proportion of the final error in thin-walled parts machining. And much effort has been made in recent years to predict and subsequently reduce the machining errors. The validated methods could be divided mainly into four categories:

- (1) Simulation by finite element method (FEM). Rai et al. [2] presented a comprehensive model based on FEM for thin-walled components milling by considering the influences of fixturing, operation sequence, tool path, and milling parameters; Jia et al. [3] developed a deflection error prediction model based on thermo-mechanical coupled effect and FEM simulation for peripheral thin-walled parts machining; Wang et al. [4] proposed a cutting force-induced error compensation method by FEM simulation and correction of milling tool path; Lazoglu et al. [5] proposed a multi-physics based FEM method to predict thin-walled parts deformation in micro-milling of Ti-6Al-4V; Liu et al. [6] considered the spring-back effect and material removal process and established a machining error prediction method based on FEM. Commercially available FEM software provides a straightforward process for deformation prediction with acceptable accuracy. However, FEM is computationally expensive and consume a large amount of computing time to produce reasonable results.
- (2) Analytical solution by mechanism analysis and modeling. Kang et al. [7] presented two analytical iterative

✉ Zhengchun Du
zcd@sjtu.edu.cn

¹ School of Mechanical Engineering, Shanghai Jiao Tong University, 800 Dongchuan RD, Minhang District, Shanghai 200240, China

method to predict milling force-induced deformation and compute the maximum surface form errors of the thin-walled workpiece, respectively; Wu et al. [8] developed a mathematical method to detect deformations of thin-walled plates based on finite difference method; Altintas et al. [9] presented a virtual prediction strategy to predict and compensate the contouring errors induced by milling forces on multi-axis machine tools; Wang et al. [10] considered the coupling effect between the axial cutting depth and workpiece deformation and proposed an accelerated convergence approach to speed up the calculation of compensation value. Mechanism models usually involve analytical solutions, in which assumptions are often made so that an analytical model is possible. This may result in difficulties of high precision prediction in complex machining conditions.

- (3) Machining parameters optimization through experiments. Koike et al. [11] proposed a cutting path optimization method by change the material removal process, tool orientation, and feed direction to minimize the workpiece machining error; Li et al. [12] focused on the effect of residual stress distribution and proposed a method to optimize the profile and magnitude of it to reduce the machining error; Yi et al. [13] analyzed the influence of fixtures on the machining process of thin plate part and used prebending method to realize error compensation; Wang et al. [14] proposed a machining sequence adjustment method to enhance the stiffness of the workpiece. Optimization of machining parameters has a wide application in industry as little understanding in the physics of the cutting process is required of the machine tool operator. However, a huge number of experiments required to find a set of optimized parameters can be time-consuming.
- (4) On-machine measurement (OMM) approach. In recent years, OMM is growing popular due to the advantage of higher efficiency compared to off-line inspection, OMM also overcomes repositioning errors that occur with off-line measurement, which affects the effectiveness of subsequent error compensation using off-line measurement data [15]. Many machining error prediction systems have been developed based on OMM for the machining error detection of the thin-walled impeller, turbine blade, etc. [16–19]. However, most of their compensation methods are based on the G code modification according to predicted errors, the low flexibility and stability of which make the high-density compensation difficult to achieve.

An important issue to be noticed is that for the OMM system, it is to treat the machine tool as a high precision coordinate measuring machine. Therefore, the volumetric errors of the machine tool generated by geometric errors of each axis

need to be modeled, measured, and compensated in advance, as well as the thermal errors induced by the deformation of machine tool components during continuous machining. Most of the above-mentioned researches ignored those two error items, which would certainly affect the measurement and machining precision.

To achieve higher prediction accuracy of thin-walled parts machining error, a comprehensive error prediction and compensation method is proposed in this paper. The rest of this paper is organized as follows. The basic process of the proposed approach is presented in Section 2. The modeling of geometric error and thermal-induced error is described in Section 3. In Section 4, the establishment process of the force-induced error model based on OMM is given. The above three error sources are integrated into a comprehensive error model in Section 5. Two sets of compensation cases are conducted to demonstrate the feasibility and consistency of the proposed approach in Section 6. Section 7 summarizes the findings and major contributions of this study.

2 Basic procedure of the comprehensive error prediction and compensation

The basic procedure of the comprehensive error prediction and compensation process is shown in Fig. 1. As introduced in Section 1, three major error sources, which are geometric error, thermal error and force-induced error, dominate the final machining accuracy of thin-walled parts. These three error items are firstly separated from the machining process for the sequential analysis and modeling. The geometric error is measured and modeled utilizing a laser interferometer with the laser bidirectional sequential step diagonal measurement method. Meanwhile, the thermal deformation of the machine tool spindle is analyzed using temperature sensors and displacement sensors to establish a thermal error prediction model. The geometric error and thermal error of the machining center need to be compensated in advance as the OMM inspection requires a high precision movement platform. After the movement accuracy of the machining center can be guaranteed, the force-induced error is measured through OMM probing. The above three error sources are finally combined to establish the comprehensive error model through the transformation of the coordinate systems, which takes real-time coordinates of the milling tooltip, real-time temperatures of specific locations as inputs and outputs the comprehensive error values, namely the real-time compensation values, for each axis at the current location and current temperature.

The compensation system is developed based on the Ethernet communication function of the NC system. It sends the real-time computed compensation values to the NC system, which are subsequently decomposed into a set of offset values for each moving axis of the machine tool. The

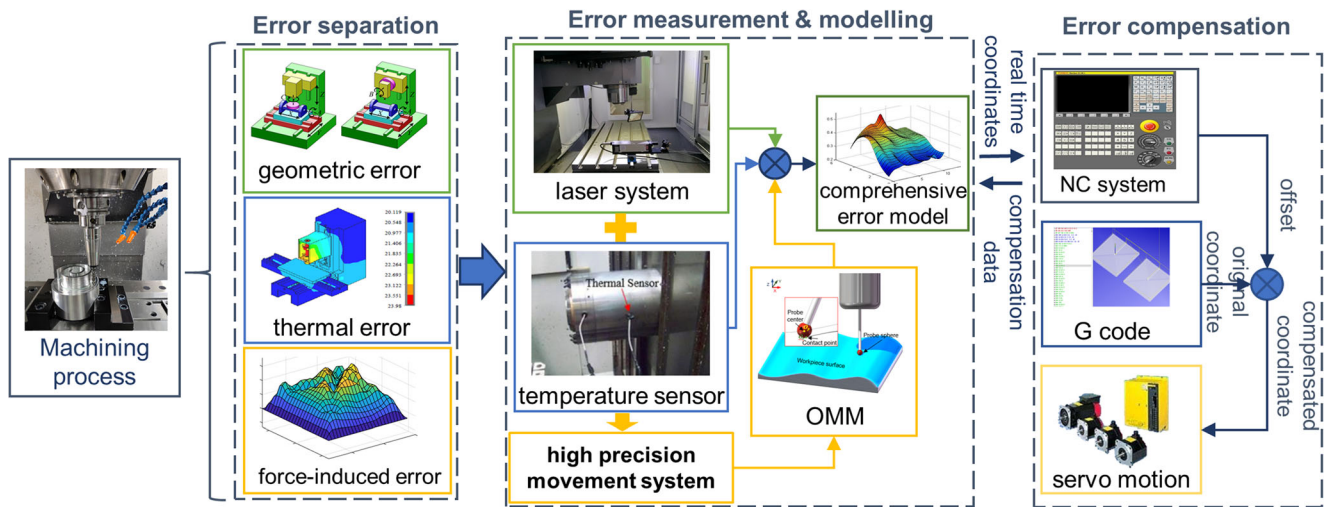


Fig. 1 Procedure of the comprehensive error prediction and compensation process

compensating offset values are written to the PLC to update the zero point of the machining coordinate system, hence realizing compensation. The above compensation cycle can be completed in a PLC scan cycle, which therefore can be considered real-time.

3 Modeling of geometric and thermal error of the machine tool

3.1 Geometric error model

As shown in Fig. 2, in ideal status, the machine table should move from O to O_i in the machine tool coordinate system. However, the actual point would be O_r due to the movement error of the machine tool. The geometric error along the Y -axis includes 3 movement errors (δ_{yy} , δ_{xy} , δ_{zy}) and 3 angular error items (ε_{xy} , ε_{yy} , ε_{zy}). There are a total of 18 error items among three motion axis and 3 squareness error items between any two of them (S_{xy} , S_{yz} , S_{xz}). According to Ref. [20], the geometric error δ_g of a typical vertical machine center

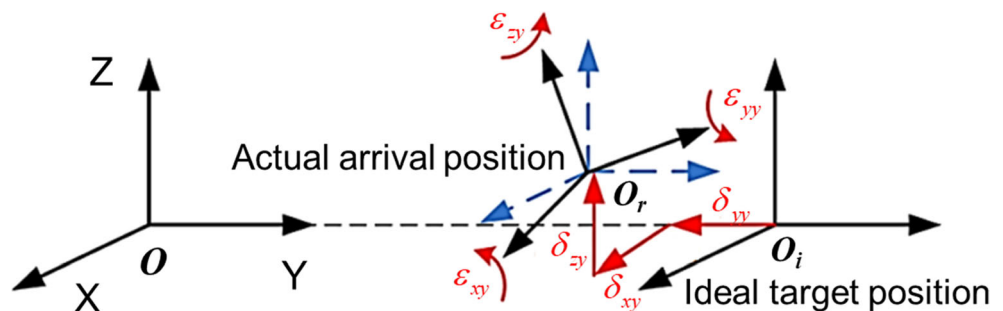
with the movement (x, y, z) can be expressed as:

$$\begin{aligned} \delta_g &= \begin{bmatrix} \Delta x_g \\ \Delta y_g \\ \Delta z_g \end{bmatrix} \\ &= \begin{bmatrix} -\delta_{xx} - \delta_{xy} + \delta_{xz} - y\varepsilon_{zx} + z\varepsilon_{yx} - y\varepsilon_{zy} + z\varepsilon_{yy} + yS_{xy} - zS_{xz} \\ -\delta_{yx} - \delta_{yy} + \delta_{yz} + x\varepsilon_{zx} + z\varepsilon_{xx} + z\varepsilon_{xy} - zS_{yz} \\ -\delta_{zx} - \delta_{zy} + \delta_{zz} + x\varepsilon_{yx} + y\varepsilon_{xx} + y\varepsilon_{xy} \end{bmatrix} \end{aligned} \tag{1}$$

where Δx_g , Δy_g , and Δz_g are the geometric error value in x , y , and z -direction of the machining center. What to be noticed is that not all the 21 geometric errors influence volumetric errors since 3 angular errors are causing no position errors. In this case, ε_{xz} , ε_{yz} , and ε_{zz} cause only orientation errors of milling tool relative to the workpiece.

The laser interferometer system, double ball bar, and the cross-grid encoder are the most commonly used devices for volumetric error measurement. Based on these devices, many direct or indirect procedures have been proposed. In this study, the laser bidirectional sequential step diagonal measurement method is adopted. By measuring and decoupling four

Fig. 2 Geometric errors of the machine tool along the Y -axis



body diagonals, all of the 18 geometric errors that result in volumetric errors of vertical machining centers can be obtained as [20]:

$$\mathbf{n} = \left(\tilde{\mathbf{T}}^T \tilde{\mathbf{T}} \right)^{-1} \tilde{\mathbf{T}}^T \mathbf{b} \quad (2)$$

where \mathbf{n} is the vector of 18 geometric errors; $\tilde{\mathbf{T}}$ is the error coefficient matrix; \mathbf{b} is the measurement data from the bidirectional sequential step diagonal measurement method.

3.2 Thermal error model

In addition to geometric errors, the thermal deformation of the major components should be modeled and compensated in advance as well to maintain the high movement precision of the machine tool. Major components including the machine tool column, bed, and spindle deform under the influence of heat sources in the machining process. The spindle deformation in the Z -axis direction contributes to the majority of the whole thermal deformation of the vertical machining center, which is focused in this study.

Seven temperature sensors are firstly placed at the machine tool bed, door of the control box, coolant tank, front end of the spindle, back end of the spindle, coolant pipe close to the spindle, and the air to measure the real-time temperatures of these locations. Meanwhile, a laser displacement sensor is installed on the machine tool table to obtain the corresponding real-time deformation data of the spindle. The key temperature locations are then selected with the following algorithm:

Firstly, a full temperature model is established using the difference between the temperature data at each location T_i and the ambient temperature T_0 , and the deformation data of the spindle in the linear form as:

$$\Delta z_t(T) = a_0 + \sum_{i=1}^6 a_i \Delta T_i \quad (3)$$

where $\Delta z_t(T)$ is the spindle deformation in the Z -axis direction, a_0 is the constant coefficient, a_i is the coefficient and ΔT_i is the temperature difference from the ambient temperature at each location.

Secondly, the impact of each ΔT_i on the spindle deformation Δz_t is examined, respectively. Each ΔT_i is substituted into Eq. (3) to calculate the corresponding spindle deformation Δz_{ti} , and then make comparisons between each Δz_{ti} and Δz_t . The temperature locations with closer results to Δz_t are selected as key location candidates.

Finally, the Pearson correlation coefficient between the selected key location candidates is checked to avoid the coupling effect between them, which will reduce the robustness and prediction accuracy of the model [21]. By comparing variable models with each other, the coolant tank, front end

of the spindle, and coolant pipe are selected as the final key temperature locations.

The thermal-induced error of the machining center, which is also the thermal expansion of the spindle in the Z -axis direction Δz_t , can be expressed with the differences between the temperatures at selected key locations and the ambient temperature as [22]:

$$\delta_t(T) = \Delta z_t = a_0 + \sum_{j=1}^3 a_j \Delta T_j \quad (4)$$

where a_0 is the constant coefficient, ΔT_j is the temperature difference between the temperature of each selected key location and the ambient temperature and a_j is the coefficient for each ΔT_j . Therefore, the thermal error can be accurately predicted with the real-time temperature values at the three optimal locations and the ambient temperature.

4 Modeling of force-induced error

Severe force-induced deformation can be expected due to the low rigidity of thin-walled parts, which is determined by cutting force or clamping force, stiffness of the workpiece and milling tool, the material removal rate, etc. and thus would require very sophisticated modeling to accurately predict the total deformation error. However, it is very straightforward to reveal the total deformation error through OMM inspection, thus the OMM system is adopted to measure the force-induced error in this study.

Touch trigger probes designed for OMM are usually installed on the spindle and they perform measurement in a similar manner as a coordinate measurement machine (CMM). Its high measurement accuracy and reliability, due to its affinity to the well understood CMM measurement principle, has made the probes fairly popular among industrial users. Locations in the machined part prone to deformation error need to be identified in advance to plan the OMM probe path. This can be achieved either by off-line quality inspection of the machine parts or with a priori knowledge of the part geometry. The probe path and the density of probing points directly affect inspection accuracy and effectiveness. In this study, a uniform equidistant distribution probe strategy is adopted due to its effectiveness and simplicity [23]. For a more accurate representation of form deviation distribution, the location and density of the sampling points can be optimized according to the part geometry, critical tolerancing zones, and a priori information of expected deformation distribution.

A machining set without compensation is firstly required to provide the machining error data for the establishment of the force-induced error model. After the inspection data is obtained, the probed surface is used to calculate the machining

errors. As is shown in Fig. 3, with respect to the designed workpiece geometry, the force-induced error can be calculated as:

$$\delta_f = \begin{bmatrix} \Delta x_f \\ \Delta y_f \\ \Delta z_f \end{bmatrix} = \begin{bmatrix} x_p \\ y_p \\ z_p \end{bmatrix} - \begin{bmatrix} x_i \\ y_i \\ z_i \end{bmatrix} \tag{5}$$

where Δx_f , Δy_f , and Δz_f are the force-induced errors, x_p , y_p , and z_p are the coordinates of the probed surface, x_i , y_i , and z_i are the coordinates of the deigned surface. Then a cubic B-spline interpolation, which has the advantages of powerful function approximation capacity and high continuity, is applied to expand the dataset, and reconstruct the machining error surface through limited discrete probing points. The modeling accuracy is determined by probing point density as more reliable interpolation can be achieved with more inspection data. However, higher probing density would significantly reduce inspection efficiency. Considering both interpolation accuracy and measurement efficiency, the probing point number is determined when it satisfies:

$$\max \left(\left[(x_r - x_i)^2 + (y_r - y_i)^2 + (z_r - z_i)^2 \right]^{1/2} \right) \leq \Delta \delta_r \tag{6}$$

where x_r , y_r , and z_r are the coordinate sets from interpolation workpiece surface; x_i , y_i , and z_i are the ideal coordinate sets from designed geometry; $\Delta \delta_r$ is the given allowable reconstruct error.

5 The comprehensive error compensation system

5.1 The comprehensive error model

According to the analysis and modeling of the three error sources in Section 3 and Section 4, the comprehensive error model can be expressed with a function of tooltip coordinates

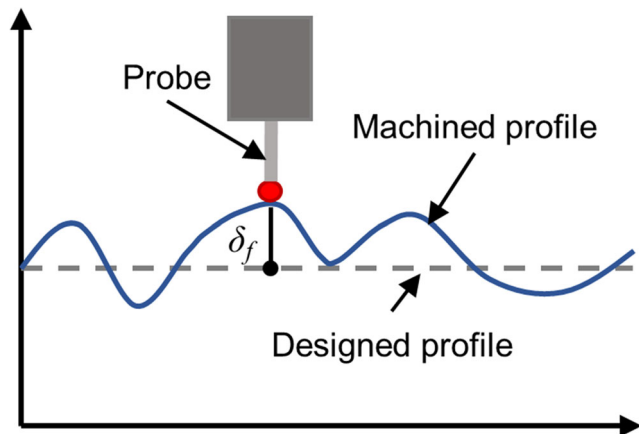


Fig. 3 OMM inspection principle

and the temperature values at selected key locations. However, the geometric error is modeled in the machine coordinate system while the force-induced error is calculated in the workpiece coordinate system. To realize the comprehensive error compensation, the three error models need to be unified into the workpiece coordinate system, which can be obtained by the translation transformation through the machine coordinate system as:

$$\delta = \begin{bmatrix} 1 & 0 & 0 & d_x \\ 0 & 1 & 0 & d_y \\ 0 & 0 & 1 & d_z \\ 0 & 0 & 0 & 1 \end{bmatrix} \cdot \begin{bmatrix} \Delta x_g + \Delta x_t \\ \Delta y_g + \Delta y_t \\ \Delta z_g + \Delta z_t \\ 1 \end{bmatrix} + \begin{bmatrix} \Delta x_f \\ \Delta y_f \\ \Delta z_f \\ 1 \end{bmatrix} \tag{7}$$

where δ is the comprehensive error; d_x , d_y , and d_z are the translation values between the two coordinates. Substituting corresponding error variables in Eq. (1), Eq. (4), and Eq. (6) to Eq. (8) yields

$$\delta(x, y, z, \Delta T_1, \Delta T_2, \Delta T_3) = \begin{bmatrix} d_x - \delta_{xx} - \delta_{xy} + \delta_{xz} - y\varepsilon_{zx} + z\varepsilon_{yx} - y\varepsilon_{zy} + z\varepsilon_{yy} + y\varepsilon_{xy} - z\varepsilon_{xz} + \Delta x_f \\ d_y - \delta_{yx} - \delta_{yy} + \delta_{yz} + x\varepsilon_{zx} + z\varepsilon_{xx} + z\varepsilon_{xy} - z\varepsilon_{yz} + \Delta y_f \\ d_z - \delta_{zx} - \delta_{zy} + \delta_{zz} + x\varepsilon_{yx} + y\varepsilon_{xx} + y\varepsilon_{xy} + a_0 + \sum_{j=1}^3 a_j \Delta T_j + \Delta z_f \end{bmatrix} \tag{8}$$

where x , y , and z are the coordinate values from the workpiece coordinate system.

5.2 Development of the real-time compensation system

The comprehensive error real-time compensation system is developed based on the Ethernet communication interface and the External Machine Zero Point Shift (EMZPS) function of the NC system, as shown in Fig. 4, which can be installed in the electrical cabinet of the machine tool. The developed system mainly consists of three parts: the main arithmetic unit, the communication interface and the EMZPS function of the NC system. The main arithmetic unit computes the comprehensive compensation value based on the established model and current machining coordinates, and then decomposed it

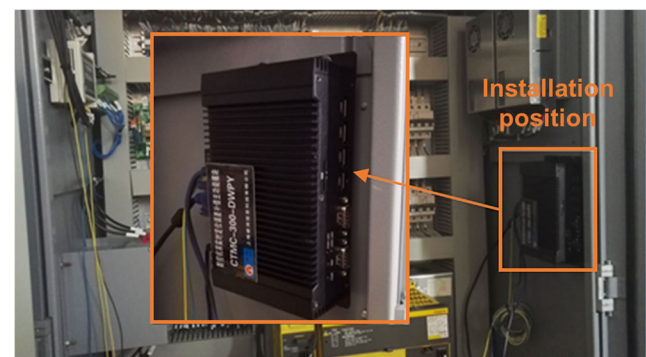


Fig. 4 The developed real-time comprehensive error compensation system

into a set of offset values for each moving axis of the machine tool. The communication interface establishes connections and transfers compensation data between the main arithmetic unit and the NC system according to corresponding commutation protocol, which is TCP/IP in this study. The EMZPS function offsets the zero point of the machining coordinate system to the computed values and then the servo motors are driven to realize compensation. The whole compensation cycle can be controlled within 20 milliseconds, which is fast enough to satisfy the machining speed in this study. After the establishment of the comprehensive error model, the system automatically compensates without modifying the NC code or system parameters during the whole machining process.

6 Case study

To validate the feasibility of the proposed comprehensive compensation method, two sets of compensation cases were conducted, the objects of which are a thin web workpiece and a valve body part, respectively.

The geometric error and the thermal-induced error are first measured and compensated to provide a high precision movement system for the OMM. As shown in Fig. 5, an Optodyne LDDM MCV-5000 laser interferometer system with a linear resolution of $\pm 0.005 \mu\text{m}$ and a system accuracy of $\pm 0.5 \text{ ppm}$ was utilized to perform the bidirectional sequential step diagonal measurement. The ambient temperature during the measurement process was 20°C . Substituting the measurement data into Eq. (2), the 18 geometric errors could be obtained simultaneously.

For the thermal-induced error, four PT100 temperature sensors, the accuracy of which was $(0.15+0.002T)^\circ\text{C}$, were placed at the coolant tank, front end of the spindle, the coolant

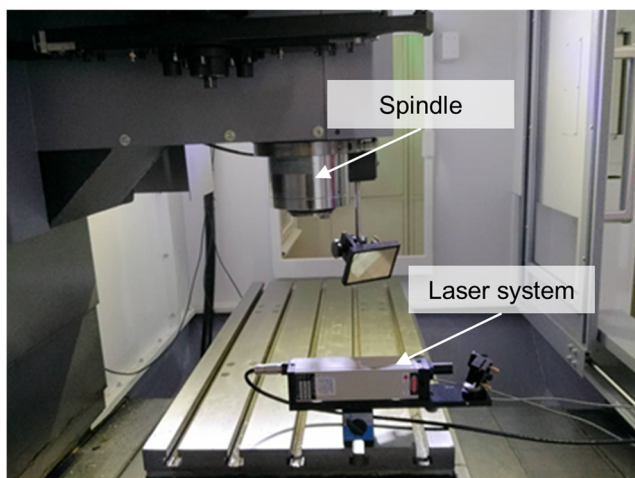


Fig. 5 Measurement of geometric error with the laser interferometer system

pipe, and the air to acquire the real-time temperature data. A Keyence IL-030 laser displacement sensor with the repeatability accuracy of $1 \mu\text{m}$ was mounted on the machine table to measure the corresponding spindle deformation. The thermal error model was established according to Eq. (4) with the measured temperature values and spindle axial deformation data.

All the 18 geometric error items were measured and compensated; however, for the thin-walled parts in this study, the Z-axis positioning error of the machining center was the dominant error item as it directly affected the probe accuracy; thus, it was investigated with emphasis. As is shown in Fig. 6, six sets of measurements for the Z-axis positioning error were conducted before and after geometric error compensation, respectively. The measurement results revealed that the average positioning error of the Z-axis was reduced from $21.9 \mu\text{m}$ to $2.4 \mu\text{m}$ with a repeatability of $1.3 \mu\text{m}$. Meanwhile, the thermal-induced error of the spindle was measured 3 times for the whole thermal equilibrium process. As is shown in Fig. 7, the average thermal-induced error was reduced from $[0, 52.5] \mu\text{m}$ to $[3.6, -7.3] \mu\text{m}$ with a repeatability of $3.6 \mu\text{m}$.

For the OMM system, it is to treat the machine tool as a high precision coordinate measuring machine, which makes the pre-control of the machine tool movement accuracy essential. Before the compensation of the abovementioned geometric error and thermal error, the long-term repetitive positioning accuracy of the Z-axis of machining center was $\sim 72 \mu\text{m}$ and the short-term repetitive positioning accuracy (within 30 mins) was $\sim 35 \mu\text{m}$, which was clearly insufficient to perform the probe task. However, after compensation, the long-term and short-time repetitive positioning accuracy were decreased to $\sim 16 \mu\text{m}$ and $\sim 6 \mu\text{m}$, respectively, which indicated that the geometric error and thermal error of the machining center were both controlled within a low level and the movement system was precision enough for the OMM inspection of force-induced error. The calibration of the probe radius and eccentricity, which need to be performed before the measurement, was conducted utilizing a ring gauge and the calibration code according to the programming guide from Renishaw.

6.1 Case 1: the thin-web part

Figure 8 shows a pocket thin web with millimeter thickness, which is the simplified model of a rocket body part. Due to the low rigidity in the pocket plane area, severe deformation under cutting forces can be expected, as is indicated in the dashed red curve in Fig. 8. After the cutting tool is disengaged from the workpiece surface, the workpiece will recover from any elastic deformation, which results in undercutting, as shown in the orange dashed curve in Fig. 8. This error source interacts with other influence factors such as material removal effect, plastic deformation, and cutting tool deflection, which would require very sophisticated modeling to accurately predict the

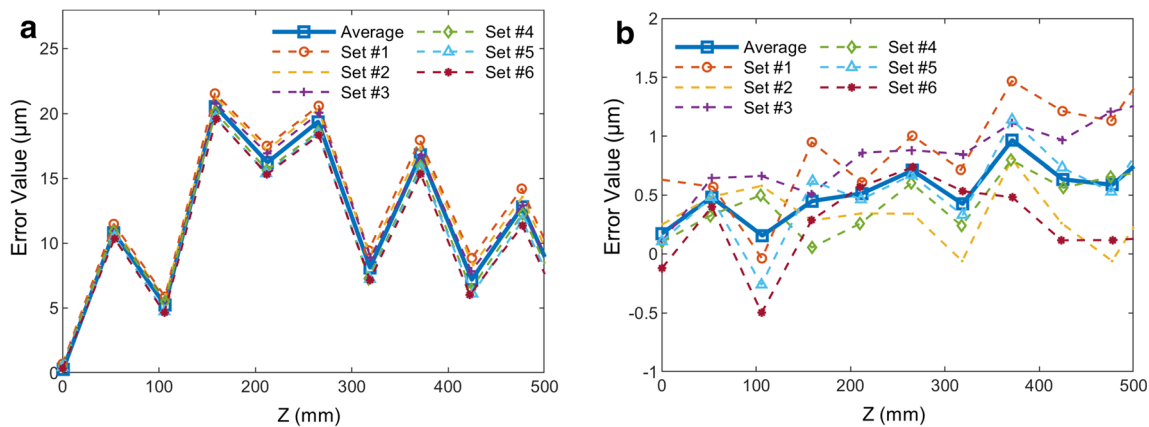


Fig. 6 a Z-axis positioning error before compensation. b Z-axis positioning error after compensation

total machining error. However, our proposed method provides a straightforward way to reveal the total machining error through OMM inspection.

6.1.1 The experiment setup

The dimension of the thin web workpiece was 250 mm × 250 mm × 4 mm. The milling tool was a four-blade flat end mill with a diameter of 12 mm and a helix angle of 30°. A VCM 850E vertical machining center with the FANUC 0i-F NC system was used to perform the machining task. The spindle speed was 6000 r/min, the radial cutting depth was 4.8 mm, and the feed rate was 0.02 mm/t.

A Renishaw RMP60 wireless touch-trigger probe with the repeatability of 1 μm was used as the OMM probe. As is shown in Fig. 9, the thin web pocket on the left side was firstly milled without compensation to compare with the compensated side, and meanwhile providing the machining error data for the establishment of the comprehensive error model. After the machining of the left pocket was finished, the probing was then implemented. In this case, the clamping force was not loaded on the sensitive area of the thin web, thus the clamping

would hardly affect the profile measurement. The probe path was designed to be six square paths, in which there were 144 uniformly distributed probe points, as shown in Fig. 8. The tool path consisted of multiple squares from inside to outside, which was similar to the probe path in Fig. 8 to make the error map near symmetrical. To ensure the repeatability of the cutting force-induced error, the inspection process was repeated three times. Then the real-time compensation was performed while milling the other thin-walled pocket on the right side for comparison. The thickness of the two thin web pockets were both machined from 4 mm to 2 mm.

6.1.2 Results and discussion

Measurement of the 144 probe points was completed within 5 minutes. The resulting machining error map of with and without compensation sets are as shown in Fig. 10. The result of three repeated inspection shows that the repeatability of the cutting force-induced error of the thin web was 1.6 μm. Figure 10a shows that the machining errors changed from around zero to negative and then back to around zero when milling from the middle to outside. This result indicates that both plastic and elastic deformation occur in the machining process because elastic deformation would only result in a single direction change of machining error. Most of the previously reported FEM-based methods [2–6] or analytical solutions [7–10] are difficult to apply to the plastic deformation prediction because of its complexity. However, our proposed OMM-based method is more robust as it is applicable for all stiffness conditions. Figure 11b shows that after the comprehensive compensation, the surface form deviation values were reduced from [−77.9, 4.8] μm to [−10.6, 18.9] μm, resulting in a reduction of maximum form error by 75.7%. The peak-to-valley form error was decreased by 64.3%. Also, the proposed compensation method changed the original two-layer machining strategy to one-layer machining, which increased the machining productivity by about 41.9%.

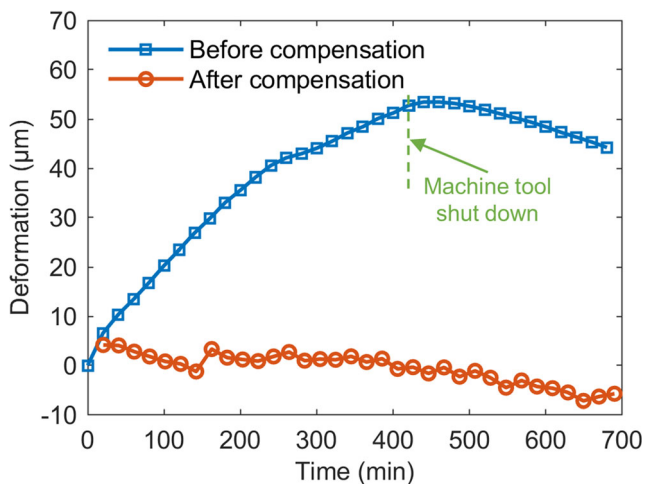
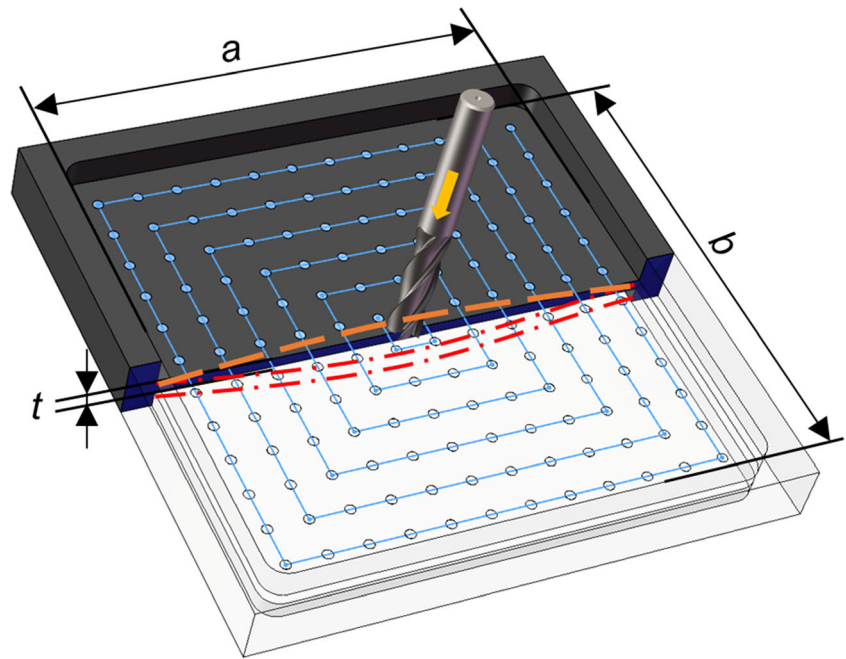


Fig. 7 Average thermal deformation before and after compensation

Fig. 8 Cutting force-induced error of the thin web part

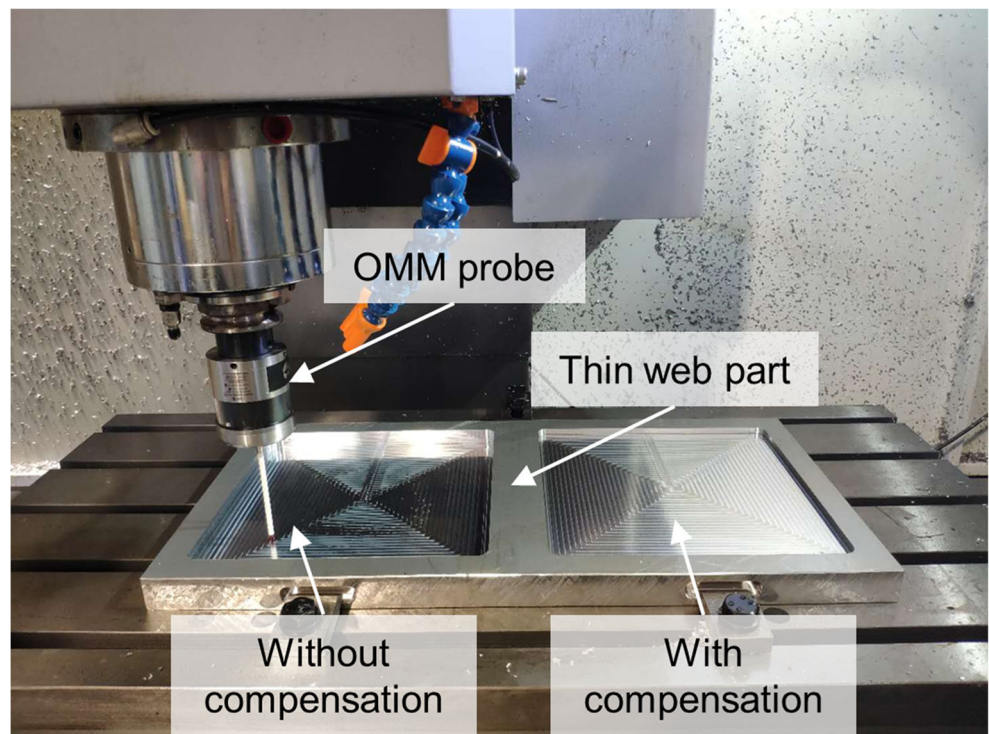


6.2 Case 2: the valve body part

Figure 12 shows an automobile gearbox valve body, which is an important part of automobile transmission parts. The valve body is designed to have many deep and complex cavities to realize specific transmission function, which meanwhile results in its low rigidity. In the machining process, the clamping force is loaded

and the valve body is expected to bend into a curved shape, as indicated in the dashed yellow curve in Fig. 11. The workpiece will rebound from elastic deformation when the clamping force is unloaded after machining and causes severe machining errors. Besides, the complex cavities make finite element analysis difficult to perform. Therefore, the proposed method is used to establish the machining error model.

Fig. 9 The OMM measurement process of the thin web part



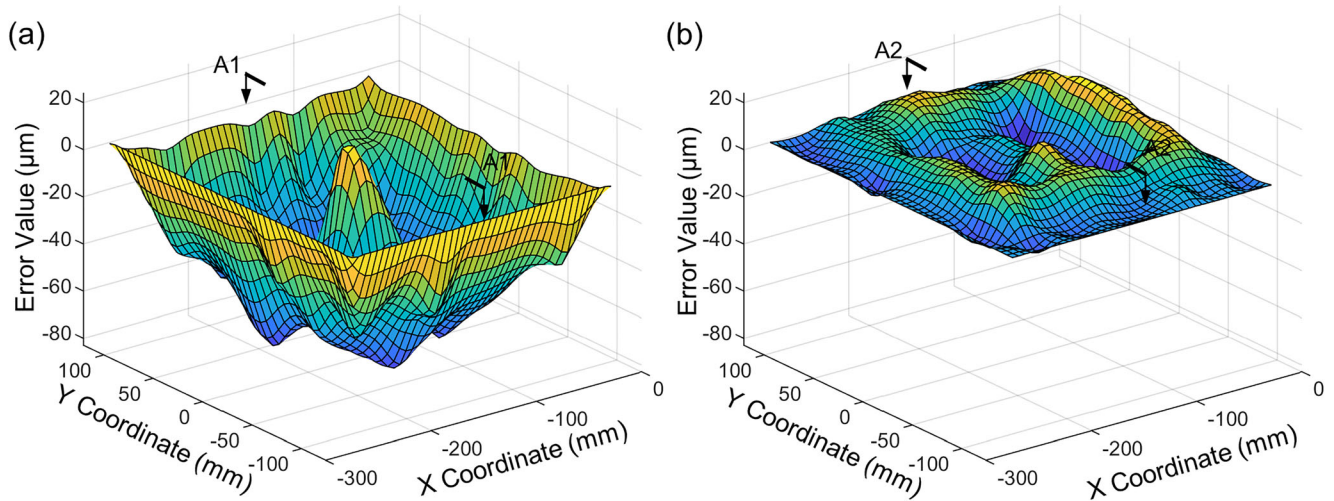


Fig. 10 a Deformed error map without compensation; b deformed error map with compensation

6.2.1 The experiment setup

The effective cutting dimension of the valve body was 285 mm × 150 mm × 38 mm, and the material was Aluminum ADC12PER. The milling tool was a six-blade disk milling cutter with a diameter of 100 mm. The machining center and the touch-trigger probe were the same as in case 1. The spindle speed was 800 r/min, the feed rate was 0.03 mm/t, and the axial cutting depth was 1.0 mm.

The machining process of the valve body was as shown in Fig. 12. The cutting path consists of three lines along y-direction under equal distance, as indicated in blue arrows in Fig. 13. The first experiment set was conducted without compensation to compare with the compensated set, and meanwhile providing the machining error data for the establishment of the comprehensive error model. After the machining was finished and the clamping force was unloaded, the OMM inspection was performed to establish the clamping force-induced error

Fig. 11 The clamping force-induced error of the valve body

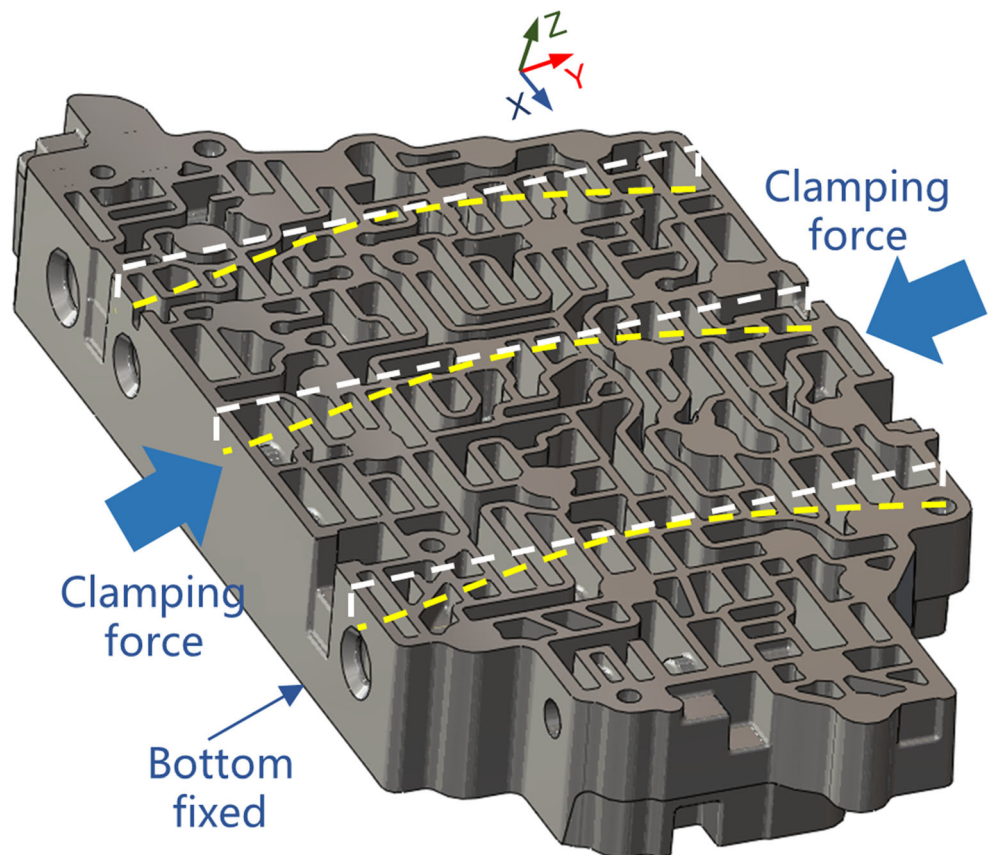
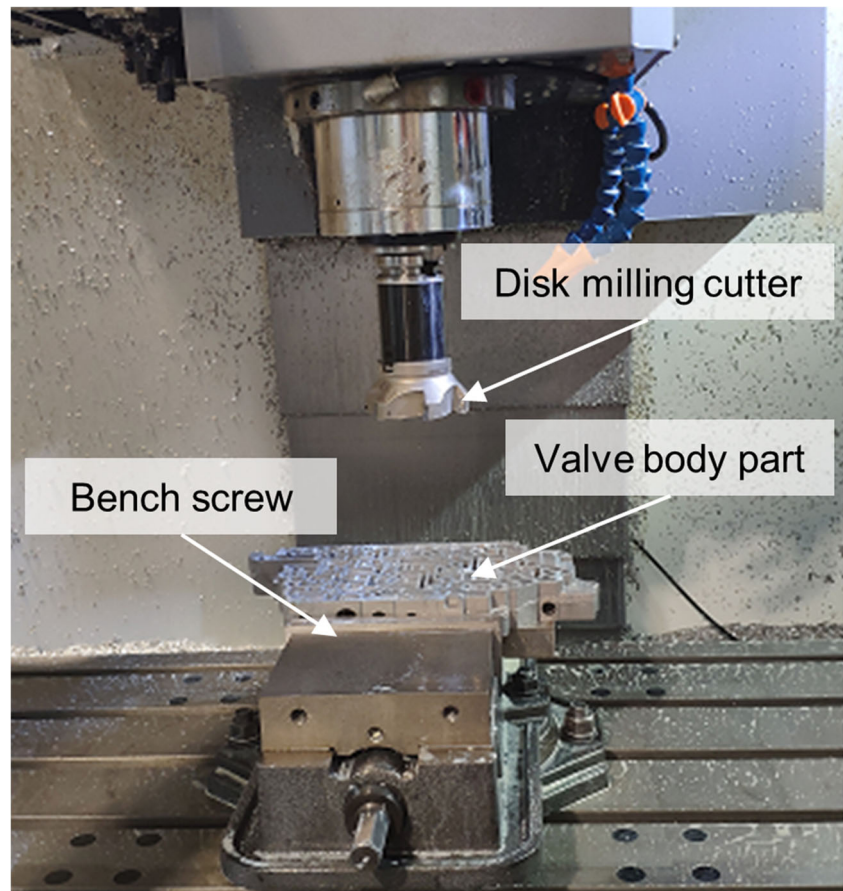


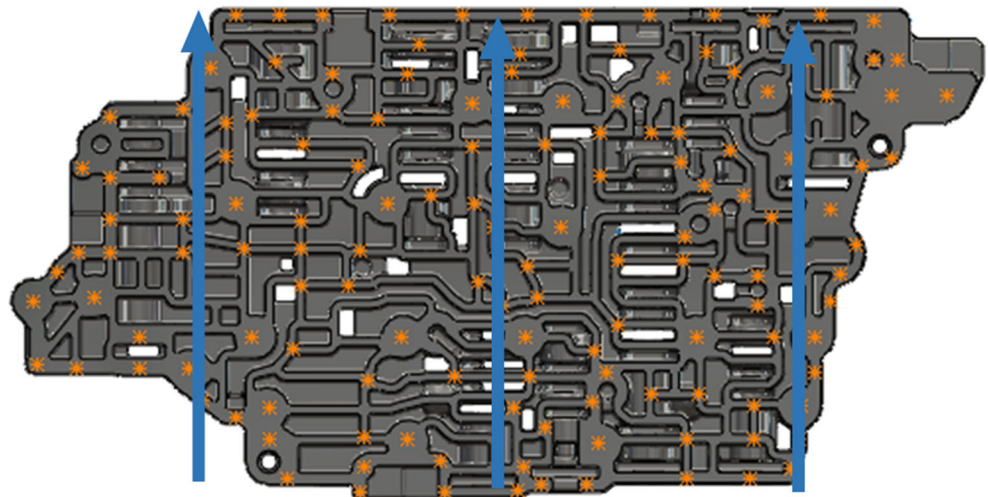
Fig. 12 Machining process of the valve body



model. According to our test, the clamping force-induced deformation of the valve body part was within elastic deformation range, which means it could completely rebound after the clamping force was unloaded. Therefore, the profile measurement of the valve body part would not be affected by the clamping. Seventy nearly uniformly distributed probe points were select from the machined surface to perform the probing, as is indicated in orange points in Fig. 13. To ensure the

repeatability of the cutting force-induced error, the inspection process was repeated three times. Then the second experiment set was carried out with the clamping force-induced error compensated to compare the compensation effect. What to be noticed is that the large radius of the cutter would result in serious undercut using the compensation path of tool center offset, thus an additional overall offset of the compensation path was applied to minimize the compensation error.

Fig. 13 The machining path and probe strategy of the valve body



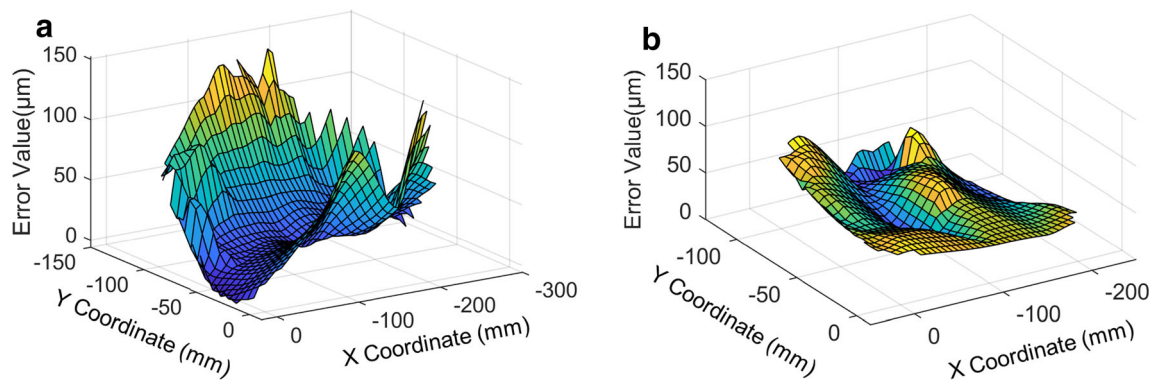


Fig. 14 **a** Deformed error map without compensation; **b** deformed error map with compensation

6.2.2 Results and discussion

The result of three repeated inspection shows that the repeatability of the clamping force-induced error of the valve body part was $1.2 \mu\text{m}$. The machining error maps of the with and without compensation sets are as shown in Fig. 14. Figure 14a shows that the machining error value varied from negative to around zero when the Y coordinate changed from the middle to both edges, which indicated that the middle of the valve body was less affected by the clamping force than the edges of the workpiece. The possible reason is that the edges of the valve body were near from the loaded clamping force and thus suffered more deformation while the deep cavities of the workpiece made the clamping force difficult to affect the middle of the workpiece. After compensation, the surface form deviation values were reduced from $[3, 148] \mu\text{m}$ to $[1, 58] \mu\text{m}$, resulting in a reduction of maximum form error by 60.8% and a reduction of peak-to-valley form error by 60.7%.

Also, the application of the proposed compensation method changed the milling strategy of the valve body from milling-CMM measurement-milling (~ 15 mins) to once milling (~ 3 mins). Considering the OMM inspection time (~ 3 mins), the machining time was decreased by 60.0%.

7 Conclusions

- (1) In this study, a comprehensive error compensation method for the thin-walled parts milling is proposed, which considers three major machining error sources including the geometric error, thermal error, and force-induced error for the first time. To perform the comprehensive error compensation, a real-time compensation system is developed based on the Ethernet communication interface and the EMZPS function of the Fanuc NC system.
- (2) The geometric error and thermal-induced error of the machining center are modeled and compensated within a low level in advance to provide a high precision movement system for the OMM inspection. The force-induced error

model is then established based on the OMM probing data. Finally, the comprehensive error model is obtained through the transformation of the coordinate systems.

- (3) Two sets of compensation cases, the objects of which are a thin web workpiece and a valve body part, respectively, are conducted to validate the proposed method. The experiment results indicate that the machining errors of both experiment sets are decreased by more than 60.7% and the machining productivity is improved by more than 41.9%. The proposed OMM-based compensation method is more robust as it performs well under complex deformation conditions that are difficult to analyze using FEM or analytical methods.
- (4) The proposed comprehensive error compensation method demonstrates the immense potential for the machining productivity and accuracy improvement of freeform surface thin-walled parts and can be further developed for the application in 5-axis machining in our future works.

Availability of data and materials All data generated or analyzed during this study are included in this article.

Author contribution Zhengchun Du was in charge of the whole trial; Guangyan Ge conducted the experiment and wrote the manuscript; Yukun Xiao assisted with sampling and laboratory analyses; Xiaobing Feng polished the manuscript and provided theoretical support on OMM detection; Jianguo Yang established the foundation of real-time error compensation technique for NC machine tools.

Funding This study was supported by the National Key R&D Program of China (Grant No. 2018YFB1701204) and National Natural Science Foundation of China (Grant No. 51975372).

Declarations

Ethics approval and consent to participate Not applicable.

Consent to publication All presentations of case reports have consent for publication.

Conflict of interest The authors declare no competing interests.

References

- Ratchev S, Liu S, Huang W, Becker AA (2006) An advanced FEA based force induced error compensation strategy in milling. *Int J Mach Tools Manuf* 46:542–551. <https://doi.org/10.1016/j.ijmactools.2005.06.003>
- Rai JK, Xirouchakis P (2008) Finite element method based machining simulation environment for analyzing part errors induced during milling of thin-walled components. *Int J Mach Tools Manuf* 48: 629–643. <https://doi.org/10.1016/j.ijmactools.2007.11.004>
- Jia Z, Guo Q, Sun Y, Guo D (2010) Redesign surface based machining strategy and method in peripheral milling of thin-walled parts. *Chinese J Mech Eng English Ed* 23:282–287. <https://doi.org/10.3901/CJME.2010.03.282>
- Wang MH, Sun Y (2014) Error prediction and compensation based on interference-free tool paths in blade milling. *Int J Adv Manuf Technol* 71:1309–1318. <https://doi.org/10.1007/s00170-013-5535-3>
- Lazoglu I, Mamedov A (2016) Deformation of thin parts in micromilling. *CIRP Ann - Manuf Technol* 65:117–120. <https://doi.org/10.1016/j.cirp.2016.04.077>
- Liu S, Shao X, Ge X, Wang D (2017) Simulation of the deformation caused by the machining cutting force on thin-walled deep cavity parts. *Int J Adv Manuf Technol* 92:3503–3517. <https://doi.org/10.1007/s00170-017-0383-1>
- Kang YG, Wang ZQ (2013) Two efficient iterative algorithms for error prediction in peripheral milling of thin-walled workpieces considering the in-cutting chip. *Int J Mach Tools Manuf* 73:55–61. <https://doi.org/10.1016/j.ijmactools.2013.06.001>
- Wu Q, Li DP, Ren L, Mo S (2016) Detecting milling deformation in 7075 aluminum alloy thin-walled plates using finite difference method. *Int J Adv Manuf Technol* 85:1291–1302. <https://doi.org/10.1007/s00170-015-8012-3>
- Altintas Y, Yang J, Kilic ZM (2019) Virtual prediction and constraint of contour errors induced by cutting force disturbances on multi-axis CNC machine tools. *CIRP Ann* 68:377–380. <https://doi.org/10.1016/j.cirp.2019.04.019>
- Wang X, Li Z, Bi Q, Zhu L, Ding H (2019) An accelerated convergence approach for real-time deformation compensation in large thin-walled parts machining. *Int J Mach Tools Manuf* 142:98–106. <https://doi.org/10.1016/j.ijmactools.2018.12.004>
- Koike Y, Matsubara A, Yamaji I (2013) Optimization of cutting path for minimizing workpiece displacement at the cutting point: changing the material removal process, feed direction, and tool orientation. *Procedia CIRP* 5:31–36. <https://doi.org/10.1016/j.procir.2013.01.006>
- Li B, Jiang X, Yang J, Liang SY (2015) Effects of depth of cut on the redistribution of residual stress and distortion during the milling of thin-walled part. *J Mater Process Technol* 216:223–233. <https://doi.org/10.1016/j.jmatprotec.2014.09.016>
- Yi W, Jiang Z, Shao W, Han X, Liu W (2015) Error compensation of thin plate-shape part with prebending method in face milling. *Chinese J Mech Eng* 28:88–95. <https://doi.org/10.3901/CJME.2014.1120.171>
- Wang J, Ibaraki S, Matsubara A (2017) A cutting sequence optimization algorithm to reduce the workpiece deformation in thin-wall machining. *Precis Eng* 50:506–514. <https://doi.org/10.1016/j.precisioneng.2017.07.006>
- Gao W, Haitjema H, Fang FZ, Leach RK, Cheung CF, Savio E, Linares JM (2019) On-machine and in-process surface metrology for precision manufacturing. *CIRP Ann* 68:843–866. <https://doi.org/10.1016/j.cirp.2019.05.005>
- Zhang Y, Zhang DH, Wu BH (2015) An adaptive approach to error compensation by on-machine measurement for precision machining of thin-walled blade. In: *IEEE/ASME International Conference on Advanced Intelligent Mechatronics*. AIM, IEEE, pp 1356–1360
- Zhao Z, Ding D, Fu Y, Xu J (2019) Measured data-driven shape-adaptive machining via spatial deformation of tool cutter positions. *Meas J Int Meas Confed* 135:244–251. <https://doi.org/10.1016/j.measurement.2018.11.051>
- Huang N, Bi Q, Wang Y, Sun C (2014) 5-Axis adaptive flank milling of flexible thin-walled parts based on the on-machine measurement. *Int J Mach Tools Manuf* 84:1–8. <https://doi.org/10.1016/j.ijmactools.2014.04.004>
- Lyssakow P, Friedrich L, Krause M, Dafnis A, Schröder KU (2020) Contactless geometric and thickness imperfection measurement system for thin-walled structures. *Meas J Int Meas Confed* 150: 107038. <https://doi.org/10.1016/j.measurement.2019.107038>
- Li H, Zhang P, Deng M, Xiang S, du Z, Yang J (2020) Volumetric error measurement and compensation of three-axis machine tools based on laser bidirectional sequential step diagonal measuring method. *Meas Sci Technol* 31:055201. <https://doi.org/10.1088/1361-6501/ab56b1>
- Li YX, Yang JG, Gelvis T, Li YY (2008) Optimization of measuring points for machine tool thermal error based on grey system theory. *Int J Adv Manuf Technol* 35:745–750. <https://doi.org/10.1007/s00170-006-0751-8>
- Liu P, Du Z, Li H et al (2020) A novel comprehensive thermal error modeling method by using the workpiece inspection data from production line for CNC machine tool. *Int J Adv Manuf Technol* 107:3921–3930. <https://doi.org/10.1007/s00170-020-05292-z>
- Talón JLH, Marín RG, García-Hernández C, Berges-Muro L, López-Gómez C, Zurdo JJM, Ortega JCC (2013) Generation of mechanizing trajectories with a minimum number of points. *Int J Adv Manuf Technol* 69:361–374. <https://doi.org/10.1007/s00170-013-5014-x>

Publisher's note Springer Nature remains neutral with regard to jurisdictional claims in published maps and institutional affiliations.